Chaos, Solitons and Fractals 139 (2020) 110061

Contents lists available at ScienceDirect

Chaos, Solitons and Fractals

Nonlinear Science, and Nonequilibrium and Complex Phenomena

journal homepage: www.elsevier.com/locate/chaos

Stimulus classification using chimera-like states in a spiking neural network

Andrey V. Andreev[a], Mikhail V. Ivanchenko[b], Alexander N. Pisarchik[a,c,*], Alexander E. Hramov[a]

[a] Neuroscience and Cognitive Technology Laboratory, Innopolis University, Universitetskaya, 1, Innopolis, 420500, Russia
[b] Department of Applied Mathematics, Mathematics of Future Technologies Center, Lobachevsky State University of Nizhny Novgorod, Gagarina Av., 23, Nizhny Novgorod, 603950, Russia
[c] Center for Biomedical Technology, Technical University of Madrid, Campus Montegancedo, Madrid, 28223, Spain

ARTICLE INFO

Article history:
Received 14 June 2020
Accepted 24 June 2020

Keywords:
Bistability
Chimera state
Classifier
Hodgkin-Huxley model
Spiking neural network

ABSTRACT

A complex network of bistable Hodgkin-Huxley (HH) neurons with excitatory coupling can exhibit a partially spiking chimera behavior. We propose to use this chimera-like state for classification of the entering stimulus amplitude in the neural network with coexisting resting and spiking states. Due to different additive noise applied to each neuron in the network, the neurons are nonidentical. Therefore, depending on the amplitude of the external current, a part of the neurons stays in the resting state, while another part oscillates. Keeping fixed the coupling strength between neurons inside the network, we train the neural network on external pulses with two different amplitudes to adjust the coupling strength between the network neurons and two output neurons. We consider two variants of the classifier, in the presence and in the absence of inhibitory coupling between output neurons, and study how the output neurons respond to the external pulses of different amplitudes. The accuracy of the proposed classifier reaches 100% when the output neurons are inhibitory coupled, so that only one of these neurons is activated.

1. Introduction

Artificial intelligence (AI) has attracted great interest of researchers, engineers and technologists due to its numerous applications in many areas, including medicine [1], radiology [2], robotics [3] and neuroscience [4]. AI helps to solve many tasks of nonlinear dynamics, for instance, nonlinear optimization [5], modeling and controlling nonlinear phenomena [6], evaluating functional connectivity [7], etc. At the same time, AI also benefits from nonlinear dynamics, for example, in such applications as artificial neural networks (ANN) [8], signal identification [9] and image encryption [10], where nonlinear dynamics approaches are successfully used to improve data recognition and classification efficiency.

In particular, ANN is a powerful machine learning method widely used for many AI applications such as approximation, classification and clustering problems, including biomedical big data, where ANNs were utilized for classification of single neuronal spikes [11, Chapter 3], multichannel EEG [12–15], MEG [16,17] and EMG [18,19] signals due to their rapidity and high efficiency. On the other hand, the majority of ANNs are based on simple functions, and therefore do not simulate dynamics of real neural networks. An alternative approach is the use of spiking neural networks (SNNs) [20] trained by biologically inspired algorithms, like, e.g., real brain circuits [21]. Nowadays, many researchers try to apply SNNs for practical purposes, for example, for speech [22] and audio-visual pattern recognition [23,24], robot controlling [25], etc. Recently, Lobov et al. [26] demonstrated that spatial or topological properties of spike-timing-dependent plasticity can be implemented as associative learning in small SNNs for controlling a mobile robot. SNNs were also used for pattern recognition of visual information recorded from a silicon retina [27], as well as in simulation of sound information processing in the auditory cortex [28,29].

Recent advances of the SNN development demonstrated that the combination of enormous computational efficiency with high classification accuracy make SNN very promissing for application in neuroscience. Specifically, in this paper we propose to explore a chimera-like state in a SNN of bistable Hodgkin-Huxley (HH) neurons for classification of an external signal amplitude. The chimera state is the coexistence of coherent and incoherent dynamics in symmetrically coupled identical dynamical units [30]. During the past decade, chimeras were found in different systems [31–34] including neural networks [35–40]. Due to their promising applications in neuroscience, this phenomenon was extensively

* Corresponding author.
E-mail address: alexander.pisarchik@ctb.upm.es (A.N. Pisarchik).

https://doi.org/10.1016/j.chaos.2020.110061
0960-0779/

investigated in complex networks of leaky integrate-and-fire neurons with excitatory coupling [37], FitzHugh-Nagumo [35,41] and Hindmarsh-Rose [36,38] neuronal oscillators, as well as in neural networks formed by physiological Hodgkin-Huxley (HH) neurons [42,43], coupled in different topological configurations (random, regular, small-world, scale-free, and modular). The experimental evidence of chimera-like states was demonstrated in a modular neuronal network based on the idea of the connectome of the C. elegans soil worm in the presence of hybrid synapses [44].

We have recently found [43] a partially spiking chimera state in a complex network of bistable Hodgkin-Huxley neurons with excitatory coupling. At certain values of the coupling strength and external current, a part of the neurons stay in the resting state, while another part oscillate. In this paper we show that this chimera state can be used for classification of external signal amplitudes.

The paper is organized as follows. In Section 2 we present the model of a scale-free network of bistable HH neurons with additive noise applied to each neuron. The spiking chimera-like state is discussed in Section 3. Then, in Section 4 we describe the proposed SNN classifier which consists of the partially spiking neural network and two output neurons. We train the classifier on external current pulses of two different amplitudes in order to adjust the coupling strength between the network neurons and two output neurons. We compare two types of the classifier's structure: with and without inhibitory coupling between the output neurons, and study dynamics of the trained SNN. We show that there is a threshold value of the pulse amplitude. If the amplitude of the input signals is below this threshold, they are classified to the first type, whereas signals whose amplitude is above the threshold are classified to the second type. Adding inhibitory couplings between the output neurons makes the classification process more stable. Finally, the results are summarized in Section 5.

2. Network model of bistable Hodgkin-Huxley neurons

We consider the HH model which describes dynamics of the membrane potential by the following system of differential equations [45]:

$$C_m\frac{dV_j}{dt} = -g_{Na}^{max}m_j^3h_j(V_j-V_{Na}) - g_K^{max}n_j^4(V_j-V_K) - g_L^{max}(V_j-V_L) + I_j^e + I_j^{syn}, \quad (1)$$

where $C_m = 1\ \mu\text{F/cm}^3$ is the capacity of cell membrane, I_j^e is an external bias current injected into j-th neuron in the network, V_j is a membrane potential of j-th neuron. The coefficients $g_{Na}^{\max} = 120\ \text{mS/cm}^2$, $g_K^{\max} = 36\ \text{mS/cm}^2$ and $g_L^{\max} = 0.3\ \text{mS/cm}^2$ respectively denote the maximal sodium, potassium and leakage conductance when all ion channels are open. $V_{Na} = 50$ mV, $V_K = -77$ mV and $V_L = -54.4$ mV are the reversal potentials for sodium, potassium and leak channels, respectively. m, n and h represent the mean ratios of open gates of specific ion channels. n^4 and m^3h are the mean portions of open potassium and sodium ion channels within a membrane patch. The dynamics of the gating variables $(x = m, n, h)$ is given as follows

$$\frac{dx_j}{dt} = \alpha_{x_j}(V_j)(1-x_j) - \beta_{x_j}(V_j)x_j + \xi_{x_j}(t), \quad (x = m, n, h), \quad (2)$$

where $\alpha_x(V)$ and $\beta_x(V)$ are the rate functions defined as [46]

$$\alpha_m(V) = \frac{0.1(25-V)}{\exp[(25-V)/10]-1}, \quad (3)$$

$$\beta_m(V) = 4\exp(-V/18), \quad (4)$$

$$\alpha_h(V) = 0.07\exp(-V/20), \quad (5)$$

$$\beta_h(V) = \frac{1}{1+\exp[(30-V)/10]}, \quad (6)$$

$$\alpha_n(V) = \frac{0.01(10-V)}{\exp[(10-V)/10]-1}, \quad (7)$$

$$\beta_n(V) = 0.125\exp(-V/80). \quad (8)$$

In Eq. (1), $\xi_x(t)$ is independent zero-mean Gaussian white noise, whose autocorrelation functions are

$$\langle\xi_{m_j}(t)\xi_{m_j}(t')\rangle = \frac{2\alpha_{m_j}\beta_{m_j}}{N_{Na}(\alpha_{m_j}+\beta_{m_j})}\delta(t-t'), \quad (9)$$

$$\langle\xi_{h_j}(t)\xi_{h_j}(t')\rangle = \frac{2\alpha_{h_j}\beta_{h_j}}{N_{Na}(\alpha_{h_j}+\beta_{h_j})}\delta(t-t'), \quad (10)$$

$$\langle\xi_{n_j}(t)\xi_{n_j}(t')\rangle = \frac{2\alpha_{n_j}\beta_{n_j}}{N_K(\alpha_{n_j}+\beta_{n_j})}\delta(t-t'). \quad (11)$$

Here, $N_{Na} = \rho_{Na}S$ and $N_K = \rho_K S$ represent the total number of sodium and potassium channels within membrane patch ($\rho_{Na} = 60\ \mu\text{m}^{-2}$ and $\rho_K = 18\ \mu\text{m}^{-2}$ being sodium and potassium channel densities, respectively) and $S = 10^{-1.7}$ is the membrane patch area of each neuron. I_j^{syn} is the total synaptic current received by j-th neuron. In this work, for simplicity we consider synaptic coupling via chemical synapses only, so that the synaptic current takes the following form

$$I_j^{syn} = \sum_{k\in neigh(j)} g_c\sigma(t-t_0^k)(E_{rev}-V_j), \quad (12)$$

where the function $\sigma(t)$ describes temporal evolution of the synaptic conductance, g_c is the maximal conductance of the synaptic channel, and t_0^k is the time at which the neighboring presynaptic k-th neuron fires. We suppose that $\sigma(t) = \text{e}^{-t/\tau_{syn}}\Theta(t)$ is proportional to the Heaviside step function $\Theta(t)$ and $\tau_{syn} = 3$ ms. The numerical calculations are carried out using the fourth-order Runge-Kutta algorithm adapted for stochastic equations with fixed integration time step $\Delta t = 10\ \mu$s.

3. Chimera-like state

For the selected values of the parameters, spiking and resting states coexist in a single HH neuron within a certain range of the external current, as seen from the bifurcation diagram in Fig. 1. In this work, we consider a scale-free network of $N = 100$ HH neurons, which initially stay in the resting state at $I_0^e = 6.25\ \mu\text{A/cm}^2$. Then, we apply a rectangular-shape external current to every network neuron (Fig. 2(a)). The pulse shape is modeled by the boxcar function

$$I^e(t) = I_0^e + I_p^e[H(t-t_0) - H(t-t_0-\Delta t)], \quad (13)$$

where I_0^e is the amplitude of the constant current, I_p^e is the amplitude of the external pulse, $H(\bullet)$ is the Heaviside step-function, $t_0 = 300$ ms is the moment of time when the pulse is applied, and $\Delta t = 300$ ms is the pulse repetition time.

In Fig. 2(a) we present the external pulse and the results of its action on the neural network without noise (Fig. 2(b)) and in the presence of noise (Fig. 2(c)). For chosen initial conditions all neurons oscillate during the transient behavior lasted from 0 to 300 ms. After transients, all neurons switch to the resting state since for the chosen value of the constant current ($I_0^e = 6.25\ \mu\text{A/cm}^2$) the neurons are monostable (see Fig. 1). When the external pulse (Eq. (13)) is applied at $t = 300$ ms, no neurons change their state in the noiseless network (Fig. 2(b)), whereas in the presence of noise a part of the neurons start to oscillate (Fig. 2(c)). The coexistence of resting and oscillating neurons is referred to as a *chimera-like state* [43]. Since each neuron has different noise, the

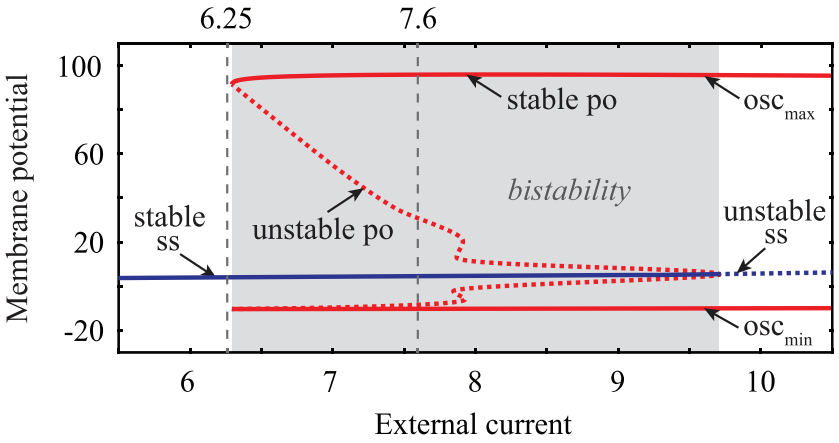

Fig. 1. Bifurcation diagram of a single HH neuron with respect to the external current used as a control parameter. Here, "ss" is a steady state, "po" is a periodic orbit, "osc_{max}" and "osc_{min}" are maximum and minimum oscillation amplitudes, respectively. The gray area indicates the bistability region with coexisting stable fixed point (blue solid line) and stable limit cycle (red solid line). The dashed red and blue lines mark unstable states. Dotted vertical grey lines indicate the values of the constant external current $I_0^e = 6.25$ μA/cm^2 and pulse current $I^e = 7.6$ μA/cm^2 used in Fig. 2. (For interpretation of the references to colour in this figure legend, the reader is referred to the web version of this article.)

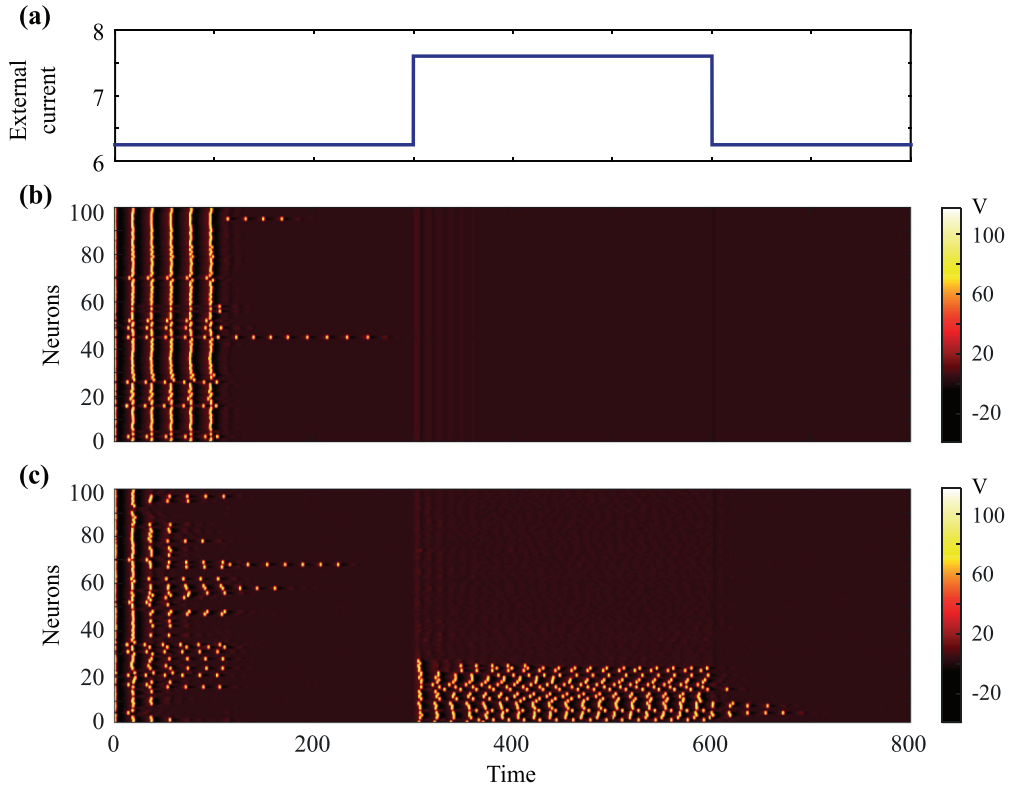

Fig. 2. (a) Rectangular-shape pulse of the external current and (b,c) spatial-temporal series of the membrane potential of the network of $N = 100$ neurons (b) without noise and (c) in the presence of noise. $I_p^e = 1.35$ μA/cm^2.

oscillators are nonidentical, and therefore we cannot consider this state as a classical chimera. When the pulse stops ($t = 600$ ms), most of the spiking neurons return back to the resting state immediately, while a small number of neurons continue to generate spikes during some transient time, but finally all neurons go to the resting state.

4. SNN Classifier

Now, we will show how the chimera-like state can serve for classification of external signal amplitudes. The proposed classifier consists of a scale-free network of $N = 100$ HH neurons and two output neurons, as shown in Fig. 3. We use the scale-free topology because this topology is characterized by the presence of nodes with extremely high degree. The adjacency matrix for this type of network is generated by the Barabási-Albert algorithm [47] that creates a graph of $N = 100$ nodes having $m = 5$ edges each. We need to train the classifier so that only one of the output neurons would be activated by a short-pulsed external current I^e applied to the main network.

Based on the previous results [43], the coupling strength between network's neurons is fixed to $g_c^m = 0.02$. Initially, the main network is not coupled with two output neurons, i.e. $g_c^{in} = 0$. Then, we train the network as follows. We apply the external pulse with

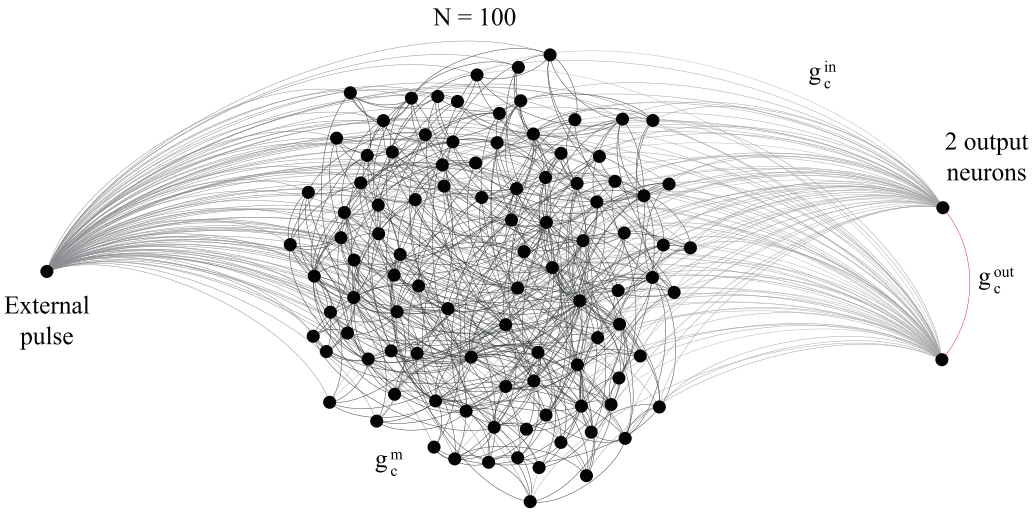

Fig. 3. Illustration of the SNN classifier. An external pulse is applied to the scale-free network of $N = 100$ Hodgkin-Huxley neurons bidirectionally coupled with strength g_c^m. All network neurons are unidirectionally coupled with two output neurons with strength g_c^{in} adjusted during the training process. The two output neurons either uncoupled or inhibitory coupled to each other with strength g_c^{out}.

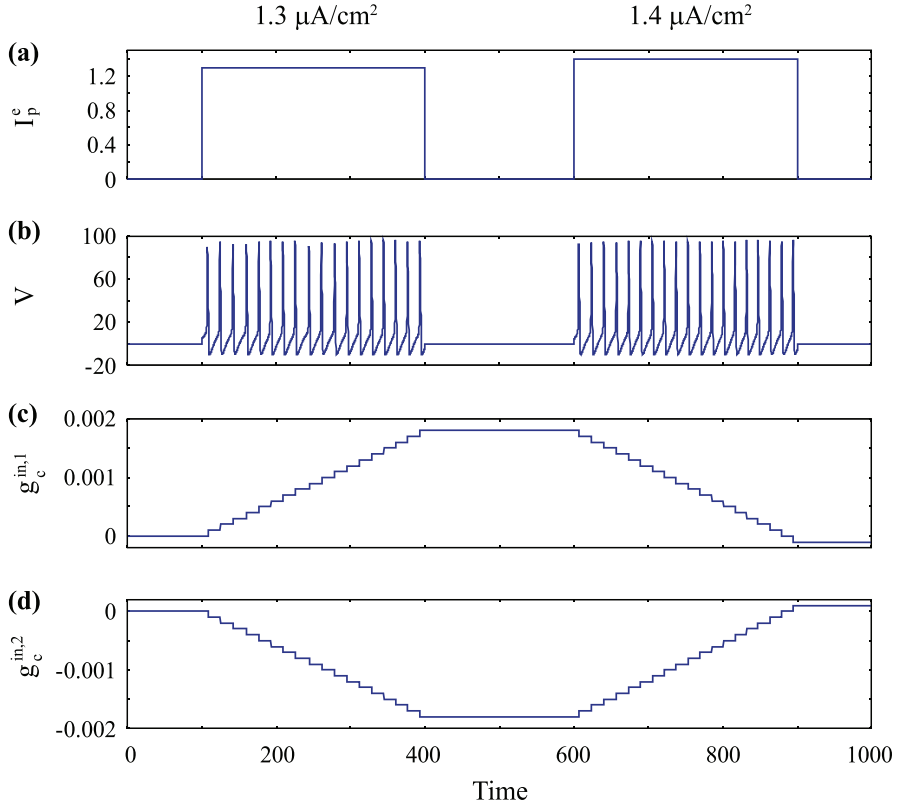

Fig. 4. Time series of (a) the external pulse amplitude, (b) membrane potential of one neuron from the main network, and (c,d) coupling strengths of this neuron with one and another output neuron.

a certain amplitude and adjust the coupling strength g_c^{in} to activate only one output neuron during the pulse, while another output neuron remains in the resting state.

Fig. 4 illustrates the training process. First, we apply the external pulse with amplitude $I_p^e = 1.3$ μA/cm^2 (Fig. 4(a)) to all neurons in the main network. Some of the neurons switch to the spiking regime as shown in Fig. 4(b). During the pulse, we increase by a small step the coupling strength between spiking neurons with one of the output neurons (Fig. 4(c)) and simultaneously decrease the coupling strength g_c^{in} with another output neuron (Fig. 4(d)). Then, we perform the training process for another pulse amplitude, namely, for $I_p^e = 1.4$ μA/cm^2 in the reverse orden, i.e., we decrease by a small step the coupling strength with the first output neuron and increase the coupling strength with the second output neuron. Since one group of the network's neurons is activated by the first pulse and another group by the second pulse, this training process should result in the situation when only one output neuron is activated by the pulses with amplitude $I_p^e > 1.4$ μA/cm^2 and another neuron with $I_p^e > 1.3$ μA/cm^2, whereas for $1.3 < I_p^e < 1.4$ μA/cm^2 both neurons are excited, but with different probability.

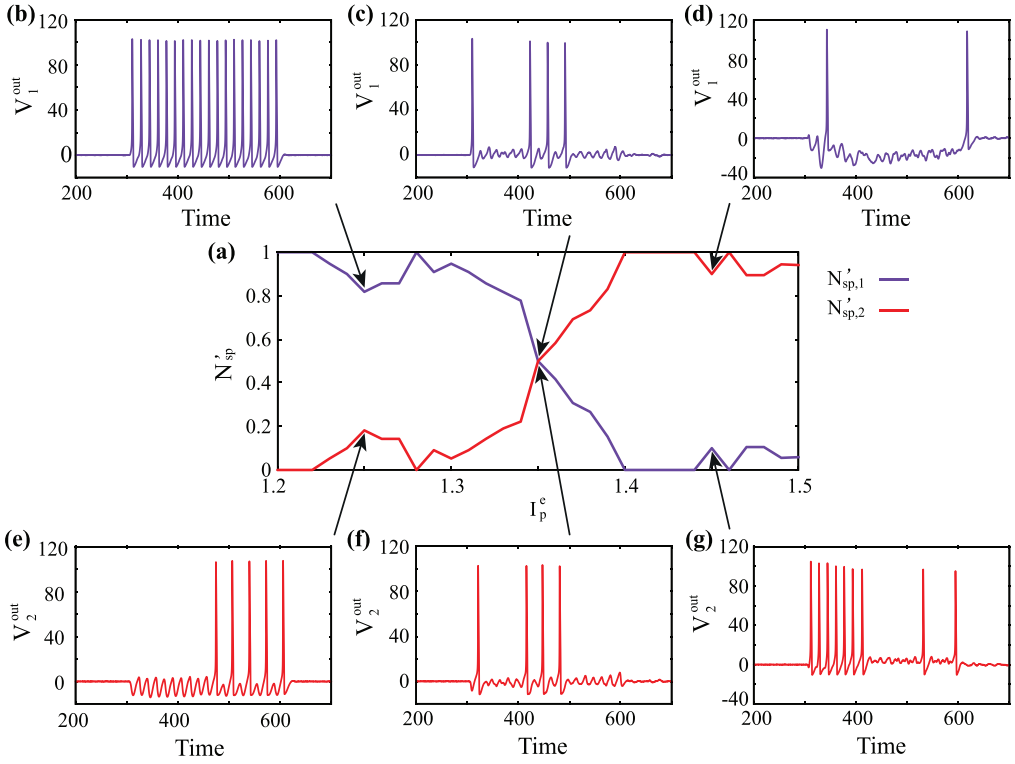

Fig. 5. (a) Normalized number of spikes of the first (blue, upper raw) and the second (red, lower raw) output neuron N'_{sp} during the pulse versus the pulse amplitude I^e_p and (b–g) time series of the membrane potential of (b–d) the first and (e–g) the second output neurons for (b,e) $I^e_p = 1.25$, (c,f) 1.35, and (d,g) 1.45 μA/cm^2. $g^{out}_c = 0$. (For interpretation of the references to colour in this figure legend, the reader is referred to the web version of this article.)

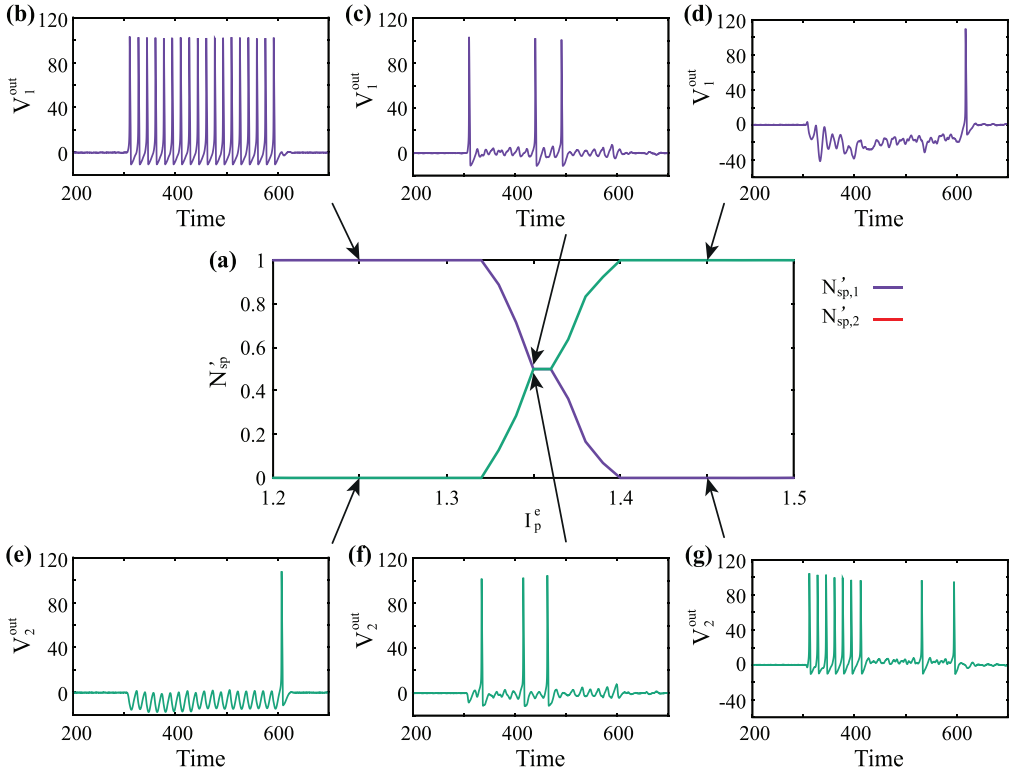

Fig. 6. (a) Normalized number of spikes of the first (blue, upper raw) and the second (red) output neuron N'_{sp} during the pulse versus the pulse amplitude I^e_p and (b–g) time series of the membrane potential of (b–d) the first and (e–g) the second output neuron for (b,e) $I^e_p = 1.25$, (c,f) 1.35, and (d,g) 1.45 μA/cm^2. $g^{out}_c = -0.15$. (For interpretation of the references to colour in this figure legend, the reader is referred to the web version of this article.)

The proposed classifier can be designed in two variants: with inhibitory coupling between the output neurons ($g_c^{out} > 0$) and without it ($g_c^{out} = 0$). The latter classifier without inhibitory coupling is trained in such a way that the first output neuron is excited by the pulse with amplitude $I_p^e = 1.3$ μA/cm^2, while the second output neuron by the pulse with $I_p^e = 1.4$ μA/cm^2. Let us study how this classifier responds to other amplitudes of the external pulsed current. The efficiency of this classifier can be estimated in terms of the normalized number of spikes generated by the output neurons

$$N'_{sp,i} = \frac{N_{sp,i}}{N_{sp,1} + N_{sp,2}}, \quad 0 \le N'_{sp,i} \le 1, \tag{14}$$

where $i = 1, 2$ is the number of the output neuron, $N_{sp,i}$ is the number of spikes generated by the i-th output neuron during the pulse ($300 < t < 600$).

Fig. 5 shows how the normalized number of spikes of the first and the second output neuron depends on the pulse amplitude. One can see that for $I_p^e = 1.2$ μA/cm^2 only the first output neuron ($i = 1$) is active, so $N'_{sp,1} = 1$. For $I_p^e = 1.25$ μA/cm^2 the second neuron is also active, but it generates only 5 spikes (Fig. 5(e)), while the first neuron generates 18 spikes during the pulse. Since we trained the network for $I_p^e = 1.3$ and 1.4 μA/cm^2, at the middle value of the pulse amplitude ($I_p^e = 1.35$ μA/cm^2) both output neurons generate equal number of spikes (Figs. 5(c,f)). A further increase in the pulse amplitude leads to the reverse situation when the second output neuron generates more spikes than the first one. One can see in Fig. 5(d) that for $I_p^e > 1.44$ μA/cm^2 the first output neuron generates 2 spikes, while the second neuron generates 9 spikes (Fig. 5(g)). Thus, the signals with $I_p^e < 1.35$ μA/cm^2 induce more pulses of the first output neuron, whereas the signals with $I_p^e > 1.35$ μA/cm^2 more pulses of the second output neuron.

Next, we will show that the introduction of inhibitory coupling between the output neurons allows avoiding uncertainty in the classification for pulses which amplitude is close to $I_p^e < 1.35$ μA/cm^2. For definiteness we fixed the coupling strength to $g_c^{out} = -0.15$. The results are shown in Fig. 6. One can see that for $I_p^e < 1.32$ μA/cm^2 only the first output neuron is active, whereas for $I_p^e > 1.4$ μA/cm^2 only the second one is active. Therefore, the uncertainty area is much narrow than in the first version of the classifier. Only for $1.32 < I_p^e < 1.4$ μA/cm^2 both neurons oscillate and generate the same number of spikes in a very narrow range of $1.35 < I_p^e < 1.36$ μA/cm^2.

Based on the above results, we can estimate the classification accuracy of our classifier. When only one output neuron is activated (for $I_p^e \le 1.32$ μA/cm^2 and $I_p^e \ge 1.4$ μA/cm^2), the accuracy is equal to 100%. However, when both neurons are simultaneously activated, the accuracy is lower, in particular, in the narrow range of the pulse amplitudes $1.35 \le I_p^e \le 1.36$ μA/cm^2 the accuracy is close to 50%.

5. Conclusion

As was previously shown, a partially spiking chimera can emerge in a complex network of bistable Hodgkin-Huxley neurons with excitatory coupling. In this paper, we have proposed to use such a chimera-like state for classification of external stimula in a spiking neural network. By adding different noise to each neuron, we make the network's neurons nonidentical, so that the external pulse current switches only a part of the neurons from the resting to the oscillatory state depending on the pulse amplitude.

The proposed SNN classifier consists of a scale-free network of 100 HH neurons and two output neurons. The classifier should be trained on external pulses with two different threshold amplitudes to adapt the coupling strength of the main network with the output neurons, so that one of the output neurons would be excited by the low-amplitude pulse, whereas another neuron by the high-amplitude pulse.

We have considered two variants of the classifier (with the presence of inhibitory coupling between the output neurons and without it) and studied how the output neurons respond to external pulses of different amplitude. For both variants, there is a threshold value for classification of the pulse amplitude. We have shown that the inhibitory coupling decreases the range of uncertainty in the stimulus amplitude classification.

We have demonstrated that the proposed classifier can achieve 100% accuracy in a wide range of external pulsed current amplitudes. The uncertainty in classification was observed within a very narrow range where both output neurons generate equal number of spikes. Such uncertainty in decision making has analogy with human perception of the bistable Necker cube which can be equally interpreted as left- or right-oriented [48,49].

Declaration of Competing Interest

The authors declare that they have no known competing financial interests or personal relationships that could have appeared to influence the work reported in this paper.

Acknowledgments

ANP and AEH thank the Russian Science Foundation (grant 17-72-30003) for support in the chimera-based classificator development. AVA and MVI acknowledge support from the Russian Foundation for Basic Research (grant 19-32-50074) for the numerical simulations.

References

[1] Topol EJ. High-performance medicine: the convergence of human and artificial intelligence. Nat Med 2019;25(1):44–56.
[2] Hosny A, Parmar C, Quackenbush J, Schwartz LH, Aerts HJ. Artificial intelligence in radiology. Nat Rev Cancer 2018;18(8):500–10.
[3] Ingrand F, Ghallab M. Robotics and artificial intelligence: a perspective on deliberation functions. AI Commun 2014;27(1):63–80.
[4] Hassabis D, Kumaran D, Summerfield C, Botvinick M. Neuroscience-inspired artificial intelligence. Neuron 2017;95:245–58.
[5] Soltani R, Sadjadi SJ, Rahnama M. Artificial intelligence combined with nonlinear optimization techniques and their application for yield curve optimization. J Ind Manag Optim 2017;13(4):1701.
[6] Scafati FT, Lavorgna M, Mancaruso E, Vaglieco BM. Artificial intelligence for modeling and control of nonlinear phenomena in internal combustion engines, in. In: Nonlinear systems and circuits in internal combustion engines. Springer; 2018. p. 1–19.
[7] Frolov N, Maksimenko V, Lüttjohann A, Koronovskii A, Hramov A. Feed-forward artificial neural network provides data-driven inference of functional connectivity. Chaos 2019;29(9):091101.
[8] Fan Y, Huang X, Wang Z, Li Y. Nonlinear dynamics and chaos in a simplified memristor-based fractional-order neural network with discontinuous memductance function. Nonlinear Dyn 2018;93(2):611–27.
[9] Carroll T. A nonlinear dynamics method for signal identification. Chaos 2007;17(2):023109.
[10] Özkaynak F. Brief review on application of nonlinear dynamics in image encryption. Nonlinear Dyn 2018;92(2):305–13.
[11] Hramov AE, Koronovskii AA, Makarov VA, Pavlov AN, Sitnikova E. Wavelets in neuroscience. Springer; 2015.
[12] Triggiani AI, Bevilacqua V, Brunetti A, Lizio R, Tattoli G, Cassano F, et al. Classification of healthy subjects and alzheimer's disease patients with dementia from cortical sources of resting state EEG rhythms: a study using artificial neural networks. Front Neurosci 2017;10:604.
[13] Hramov AE, Maksimenko VA, Pchelintseva SV, Runnova AE, V Grubov V, Musatov VY, et al. Classifying the perceptual interpretations of a bistable image using EEG and artificial neural networks. Front Neurosci 2017;11:674.
[14] Maksimenko VA, Kurkin SA, Pitsik EN, Musatov VY, Runnova AE, Efremova TY, et al. Artificial neural network classification of motor-related EEG: an increase in classification accuracy by reducing signal complexity. Complexity 2018;2018:9385947.
[15] Hramov AE, Maksimenko V, Koronovskii A, Runnova AE, Zhuravlev M, Pisarchik AN, Kurths J. Percept-related EEG classification using machine learning approach and features of functional brain connectivity. Chaos 2019;29(9):093110.

[16] Hramov AE, Frolov NS, Maksimenko VA, Makarov VV, Koronovskii AA, Garcia–Prieto J, Antón-Toro LF, Maestú F, Pisarchik AN. Artificial neural network detects human uncertainty. Chaos 2018;28(3):033607.
[17] Hramov A.E., Pisarchik A.N., Sahu M., Sinha G.R.. Artificial neuronal networks for classification of brain states under visual stimuli processing: EEG and MEG studies. In: Brain and behavior computing. CRC Press of Taylor & Francis Group (in press);
[18] Roche AD, Rehbaum H, Farina D, Aszmann OC. Prosthetic myoelectric control strategies: a clinical perspective. Curr Surg Rep 2014;2(3):44.
[19] Hahne JM, Biessmann F, Jiang N, Rehbaum H, Farina D, Meinecke FC, et al. Linear and nonlinear regression techniques for simultaneous and proportional myoelectric control. IEEE Trans Neural Syst Rehabil Eng 2014;22(2):269–79.
[20] Quiroga RQ, Panzeri S. Principles of neural coding. CRC Press; 2013.
[21] Lobov SA, Chernyshov AV, Krilova NP, Shamshin MO, Kazantsev VB. Competitive learning in a spiking neural network: towards an intelligent pattern classifier. Sensors 2020;20(2):500.
[22] Yu D, Deng L. Automatic speech recognition. Springer; 2016.
[23] Kasabov NK. Evolving connectionist systems: the knowledge engineering approach. Springer Science & Business Media; 2007.
[24] Hossain MS, Muhammad G. Emotion recognition using deep learning approach from audio–visual emotional big data. Inf Fusion 2019;49:69–78.
[25] Bing Z, Meschede C, Röhrbein F, Huang K, Knoll AC. A survey of robotics control based on learning-inspired spiking neural networks,. Front Neurorobot 2018;12:35.
[26] Lobov SA, Mikhaylov AN, Shamshin M, Makarov VA, Kazantsev VB. Spatial properties of STDP in a self-learning spiking neural network enable controlling a mobile robot. Front Neurosci 2020;14:88.
[27] Bichler O, Querlioz D, Thorpe SJ, Bourgoin J-P, Gamrat C. Unsupervised features extraction from asynchronous silicon retina through spike-timing-dependent plasticity. In: The 2011 international joint conference on neural networks. IEEE; 2011. p. 859–66.
[28] Voutsas K, Adamy J. A biologically inspired spiking neural network for sound source lateralization. IEEE Trans Neural Networks 2007;18(6):1785–99.
[29] Wang G, Pavel M. A spiking neuron representation of auditory signals. In: Proceedings of the 2005 IEEE international joint conference on neural networks, Vol. 1. IEEE; 2005. p. 416–21.
[30] Kuramoto Y, Battogtokh D. Coexistence of coherence and incoherence in nonlocally coupled phase oscillators. Nonlinear Phenom Complex Syst 2002;5(4):380–5.
[31] Omelchenko I, Maistrenko Y, Hövel P, Schöll E. Loss of coherence in dynamical networks: spatial chaos and chimera states. Phys Rev Lett 2001;106:234102.
[32] Makarov VV, Kundu S, Kirsanov DV, Frolov NS, Maksimenko VA, Ghosh D, et al. Multiscale interaction promotes chimera states in complex networks. Commun Nonlinear Sci Numer Simul 2019;71:118–29.
[33] Kapitaniak T, Kuzma P, Wojewoda J, Czolczynski K, Maistrenko Y. Imperfect chimera states for coupled pendula. Sci Rep 2014;4:6379.
[34] Maksimenko VA, Makarov VV, Bera BK, Ghosh D, Dana SK, Goremyko MV, et al. Excitation and suppression of chimera states by multiplexing. Phys Rev E 2016;94(5):052205.
[35] Hövel P, Omelchenko I. Multi-chimera states in fitzhugh-nagumo oscillators. BMC Neuroscience 2013;14. P303
[36] Hizanidis J, Kanas VG, Bezerianos A, Bountis T. Chimera states in networks of nonlocally coupled hindmarsh-rose neuron models. Int J Bifurcation Chaos 2014;24(3):1450030.
[37] Tsigkri-DeSmedt ND, Hizanidis J, Schöll E, Hövel P, Provata A. Chimeras in leaky integrate-and-fire neural networks: effects of reflecting connectivities. Eur Phys J B 2017;90(7):139.
[38] Bandyopadhyay A, Kar S. Impact of network structure on synchronization of hindmarsh–rose neurons coupled in structured network. Appl Math Comput 2018;333:194.
[39] Majhi S, Bera BK, Ghosh D, Perc M. Chimera states in neuronal networks: a review. Phys Life Rev 2019;28:100–21.
[40] Bera BK, Rakshit S, Ghosh D, Kurths J. Spike chimera states and firing regularities in neuronal hypernetworks. Chaos 2019;29(5):053115.
[41] Omelchenko I, Provata A, Hizanidis J, Schöll E, Hövel P. Robustness of chimera states for coupled fitzhugh-nagumo oscillators,. Phys Rev E 2015;91(2):022917.
[42] Glaze TA, Lewis S, Bahar S. Chimera states in a hodgkin-huxley model of thermally sensitive neurons. Chaos 2016;26:083119.
[43] Andreev A, Frolov N, Pisarchik A, Hramov A. Chimera state in complex networks of bistable hodgkin-huxley neurons. Phys Rev E 2019;100(2):022224.
[44] Hizanidis J, Kouvaris NE, Zamora-López G, Díaz-Guilera A, Antonopoulos CG. Chimera-like states in modular neural networks. Sci Rep 2016;6:19845.
[45] Hodgkin A, Huxley A. A quantitative description of membrane current and its application to conduction and excitation in nerve. J Physiol 1952;117:500–44.
[46] Pankratova EV, Polovinkin AV. Resonant activation in a stochastic hodgkin-huxley model: interplay between noise and suprathreshold driving effects. Eur Phys J B 2005;45:391. doi:10.1140/epjb/e2005-00187-2.
[47] Barabási A-L, Albert R. Emergence of scaling in random networks,. Science 1999;286(5439):509–12. doi:10.1126/science.286.5439.509.
[48] Pisarchik AN, Jaimes-Reátegui R, Magallón-García CA, Castillo-Morales CO. Critical slowing down and noise-induced intermittency in bistable perception: bifurcation analysis. Biol Cybern 2014;108(4):397–404.
[49] Runnova AE, Hramov AE, Grubov VV, Koronovskii AA, Kurovskaya MK, Pisarchik AN. Theoretical background and experimental measurements of human brain noise intensity in perception of ambiguous images. Chaos Solitons Fractals 2016;93:201–6.